Supplementary Information

From Atomic Modification to Structure Engineering: Layered NiCo-MnO₂ with Ultrafast Kinetics and Optimized Stress Distribution for Aqueous Zinc Ions Storage

Junyi Yin[‡], Runxi Zhu[∥,2], Linghan Xia[‡], Haoliang Liu[‡], Yuan Gao[‡], Zihan Gan[‡], Xiang Feng[‡], Minghui Wang[‡], Guodong Meng[‡], Yaqiong Su[∥,2], Yonghong Cheng*[‡] and Xin Xu*[‡]*

[‡]State Key Laboratory of Electrical Insulation and Power Equipment, School of Electrical Engineering, Xi'an Jiaotong University, Xi'an 710049, China

[∥]Engineering Research Center of Energy Storage Materials and Devices, Ministry of Education, Xi'an Jiaotong University, Xi'an 710049, China

[2]Xi'an Key Laboratory of Sustainable Energy Materials Chemistry, School of Chemistry, Xi'an Jiaotong University, Xi'an 710049, China

*Email: yqsu1989@xjtu.edu.cn (Y. Su); cyh@mail.xjtu.edu.cn (Y. Cheng); xu.xin@xjtu.edu.cn (X. Xu)

Experimental Section

Material Synthesis

Synthesis of NiCo-PBA nanocubes: The NiCo–Prussian blue analog (PBA) nanocubes were synthesized via coprecipitation. First, 149.3 mg of nickel acetate tetrahydrate and 264.7 mg of sodium citrate were dissolved in 20 mL of deionized (DI) water to form solution A. Then, 131.7 mg $K_3[Co(CN)_6]$ was dissolved in 20 mL of DI water to form solution B. Afterward, solutions A and B were mixed with constant stirring for 3 min and then left to stand at room temperature for 24 h. The precipitates were centrifuged at 8000 rpm, washed several times with DI water and ethanol, and then oven-dried at 60 °C.

Synthesis of Ni-Co-MnO₂: First, 30 mg of NiCo–PBA nanocubes, 316 mg of $KMnO_4$, and 35 mL of DI water were mixed to form a uniform suspension. The mixture was stirred and sonicated for 30 min and then transferred to a 50 mL Teflon-lined autoclave. The autoclave was placed in an oven at 180 °C for 3 h, and a brownish precipitate was collected via high-speed centrifugation at 8000 rpm. The precipitate was washed several times with DI water and ethanol and oven-dried at 60 °C to obtain the final product.

Synthesis of pristine MnO₂: 316 mg of $KMnO_4$, and 35 mL of DI water were mixed to form a uniform suspension. The mixture was stirred and sonicated for 30 min and then transferred to a 50 mL Teflon-lined autoclave. The autoclave was placed in an oven at 180 °C for 3 h, and a brownish precipitate was collected via high-speed

centrifugation at 8000 rpm. The precipitate was washed several times with DI water and ethanol and oven-dried at 60 °C to obtain the final product.

Materials Characterization

The morphologies of the materials, elemental maps, and selected-area electron diffraction patterns were obtained via SEM (ZEISS, Gemini 500) and TEM (Talos F200X) coupled with energy-dispersive X-ray spectroscopy. X-ray diffraction analysis was conducted using the Bruker D8 Advance with Cu Kα radiation ($\lambda = 1.54184$ Å). X-ray photoelectron spectroscopy analysis was conducted using the AXIS Ultrabold spectrometer. Raman spectra were collected using the Renishaw Raman RE01 spectrometer with a 633 nm laser. The nitrogen adsorption–desorption isotherms and pore-size distributions of the samples were obtained using an automatic physical adsorption instrument (ASAP 2020 Plus HD88).

Electrochemical Measurements

The coin cells (CR 2025) were assembled in an air atmosphere. The working electrode was composed of 70% as-prepared active material, 20% conductive agent (super P, Timcal), and 10% polymer binder (polyvinylidene fluoride, Macklin). To prepare the working electrode, the slurry was pasted onto a stainless-steel foil (weighed previously) and vacuum-dried at 80 °C for 12 h. Afterward, the stainless steel foil was reweighed to calculate the area density of the active material. The mass loading of the active materials was 1.0–2.0 mg cm^{-2}. The electrolyte used was 2 M $ZnSO_4$ and 0.1 M $MnSO_4$ aqueous solution with 10 mM glucose additive. A Zn foil served as both the counter electrode and the reference electrode. Galvanostatic charge–discharge and

galvanostatic intermittent titration technique tests were conducted on a Neware battery tester. A cyclic voltammetry test was performed at a scan rate of 0.8–1.8 mV s^{-1} using an electrochemical workstation (CHI 1040C, CH Instruments, Inc.). Nyquist plots were obtained using a CHI 760E workstation (CH Instruments, Inc.), with frequency ranges of 0.01 Hz to 100 MHz.

Calculation of diffusion and capacitive-controlled capacities

According to previous studies, a qualitative relationship (Equation S1) exists between the peak current (i) and the scanning rate (v) in cyclic voltammetry curves:[1,2]

$$i(v) = av^b \tag{1}$$

where the b value is calculated using the fitted slope between $\log(i)$ and $\log(v)$; this value is crucial in determining the diffusion and capacitive-controlled contributions in the Zn^{2+} storage process. Typically, a b value of 1 indicates a capacitive-controlled effect to deliver a high rate capability, while a b value of 0.5 corresponds to a diffusion-limited charge storage process, in which the electrode needs sufficient time to complete the charge storage progress. Furthermore, using Equation S2, we quantitatively calculated the pseudocapacitive contribution proportion (k_1v) and the diffusion current contribution ($k_2v^{1/2}$):[3]

$$i(v) = i_1 + i_2 = k_1v + k_2v^{1/2} \tag{2}$$

Calculation of the Diffusion Coefficients of Zinc Ions

The diffusion coefficients of zinc ions ($D_{Zn^{2+}}$) in NCMO and pristine MnO$_2$ were calculated using Equation S3:

$$D_{Zn^{2+}} = 4(n_mV_m)^2S^{-2}(\pi\tau)^{-1}(\varDelta E_s)^2(\varDelta E_\tau)^{-2} \tag{3}$$

where τ (s) represents the constant current pulse time; n_m (g mol^{-1}) and V_m (cm^3 mol^{-1}) represent the number of moles and the molar volume of the active materials, respectively; S (cm^2) represents the contact area of the electrode; and ΔE_s and ΔE_τ denote the potential change triggered by the pulse and the constant current charge–discharge, respectively. A current density of 100 mA g^{-1} was applied to the cells, with $\tau = 10$ min, and then the cells were allowed to stand for 600 s without current application.

COMSOL Simulation Methods

The simulations were conducted using the COMSOL 5.6 AC/DC module, and the 3D model parameters were set according to the scanning electron microscopy (SEM) and transmission electron microscopy (TEM) images. In the setup of the NCMO model, the side length of the cubic framework was 300 nm, and the width of the facial nanosheets was 100 nm, with a thickness of 3 nm. In the MO model, the nanosheets were 3 nm thick and 300 nm wide. The current flows were set across the 3D models.

Density-Functional Theory Calculation Methods

Density-functional theory (DFT) calculations were performed using the Vienna Ab initio Simulation Package (VASP). The ion–electron interactions were described via the projector augmented-wave method with frozen-core approximation. The energies and geometries of the most stable configurations were obtained through the minimization of the total energy with respect to geometry. The exchange–correlation energy was described via generalized gradient approximation calculations using the spin-polarized Perdew–Burke–Ernzerhof functional. The Kohn–Sham valence states

were expanded in a plane-wave basis set with a cut-off energy of 400 eV. The size of supercell is a=8.823 Å, b=11.372 Å, c=18.967 Å. A Monkhorst–Pack $3 \times 3 \times 1$ mesh was used for the Brillouin zone integration. The van der Waals interaction was described via the dispersion correction method DFT-D3 with Becke–Johnson damping. The DFT+U approach was used to improve the description of localized states in 3d orbitals, where U is a Hubbard-like term describing on-site Coulombic interactions. For Mn, Co, and Ni, U value is 4.9, 3.0 and 6.5 eV, respectively. The U values are obtained according to the previous reported works.[4-6] The initial and final position of the Zn^{2+} is Co-top and Ni-top. In the case of the doped structure, Zn^{2+} is absorbed on the top of Co (Co-top), and the left and right sides of Zn^{2+} are both the dopant Ni. Moreover, the different adsorption sites were considered and the calculation results are shown as below: E_{ads}(Co-top) = -1.95 eV, E_{ads}(Ni-top) = -1.93 eV.

The adsorption energy between Zn and substrate is defined by Equation S4:

$$E_{ads} = E_{(Zn\text{-}substrate)} - E_{(Zn)} - E_{(substrate)} \tag{4}$$

where, in this work, E_{ads} is the adsorption energy between Zn and substrate (MO or NCMO), $E_{(Zn\text{-}substrate)}$ is the energy of adsorption structure of Zn and substrate. $E_{(Zn)}$ is the energy of Zn and $E_{(substrate)}$ is the energy of substrate.

The calculation of charge density difference of the Zn-MO and Zn-NCMO model is to obtain not only the electron flow directions, but also the change of electron density and the formation of chemical bonds during the interaction process between the two fragments of substrate and Zn. The calculation principle of charge density difference is displayed in the following Equation S5:

$$\Delta\rho = \rho_{AB} - \rho_A - \rho_B \tag{5}$$

where, in this work, $\triangle\rho$ is the charge density difference of the whole Zn-MO or Zn-NCMO system, ρ_{AB} is the charge density of Zn-MO or Zn-NCMO system, ρ_A is the charge density of substrate (MO or NCMO) and ρ_B is the charge density of adsorbate (Zn). The calculation is to reveal the charges redistribution between the MO/NCMO and Zn after the intercalation of adsorbate, as well as the charges loss during the transition of the entire system from atomic state to ionic state.

Supplementary Tables and Figures:
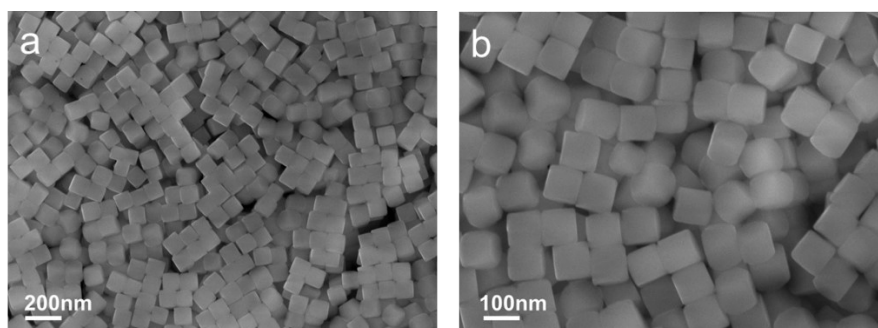
Figure S1. SEM images of NiCo–PBA nanocubes.
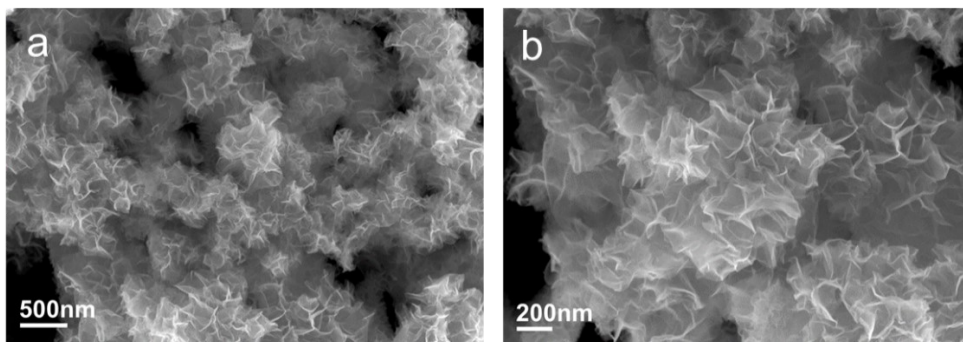
Figure S2. SEM images of MnO_2 nanosheets.
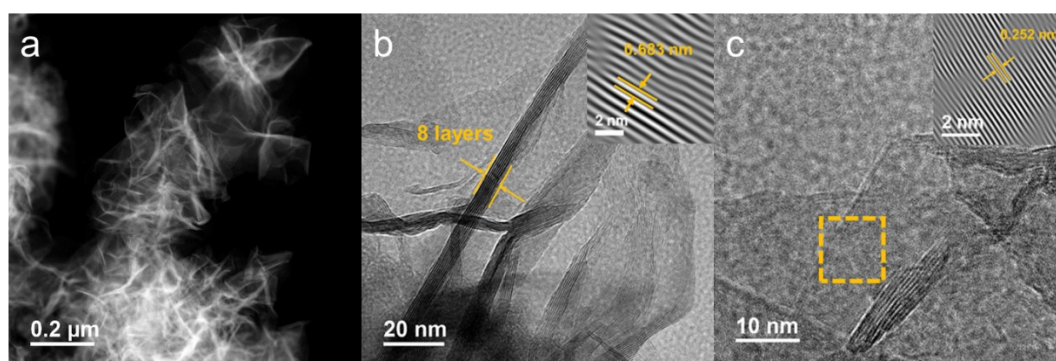
Figure S3. High-angle annular dark-field images of pure MnO_2 (inset: inverse fast-Fourier transform patterns).
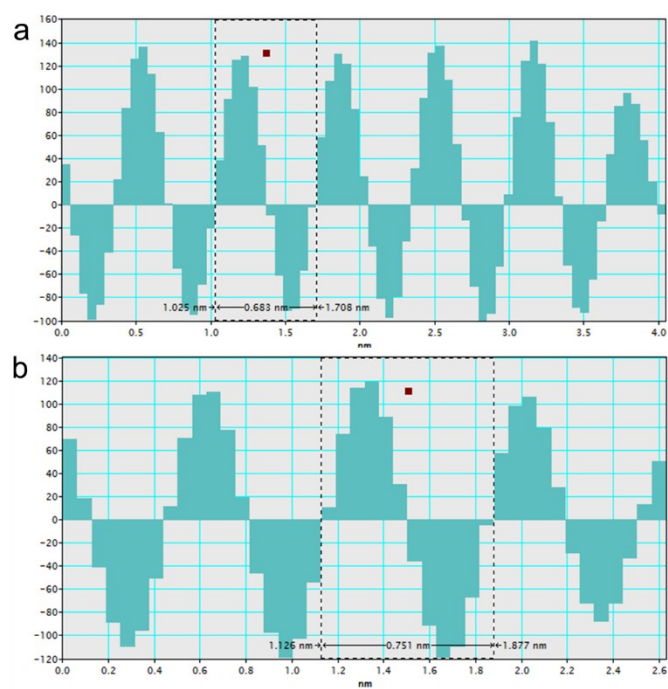
Figure S4. The interlayer distance measurements of pure MnO_2 (a) and NCMO (b).
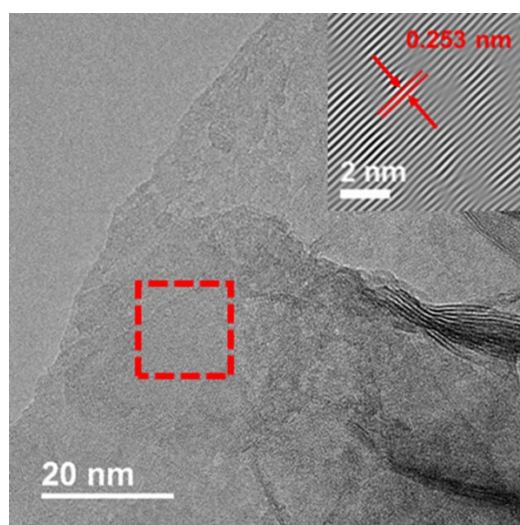
Figure S5. High-resolution TEM images of NCMO (inset: inverse fast-Fourier transform patterns).
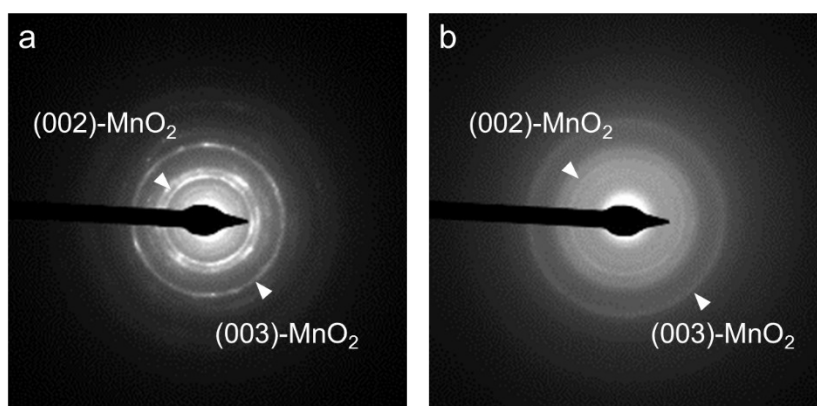
Figure S6. Selected-area electron diffraction images of pure MnO_2 (a) and NCMO (b)

samples.
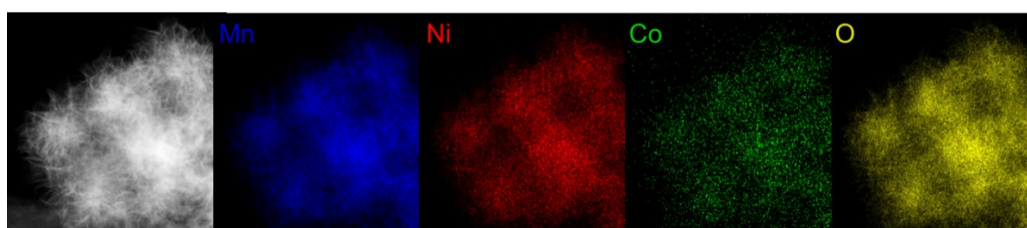
Figure S7. HAADF image and corresponding element mapping of NCMO sample.
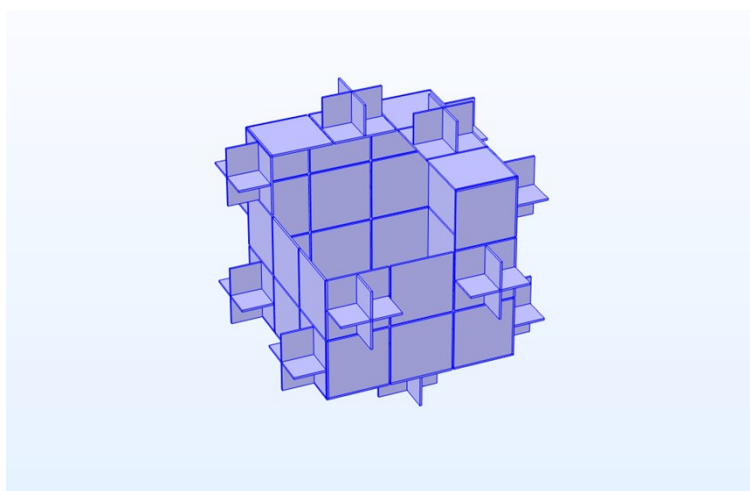
Figure S8. The finite-element model construction of NCMO.
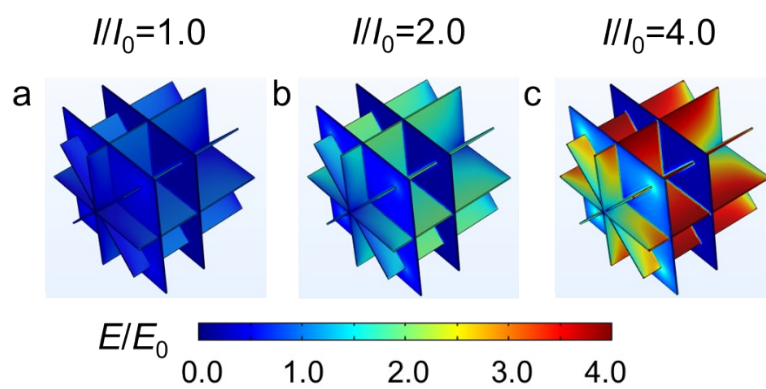
Figure S9. Electric field intensity distributions for MO models at current densities of

I_0, $2I_0$, and $4I_0$.
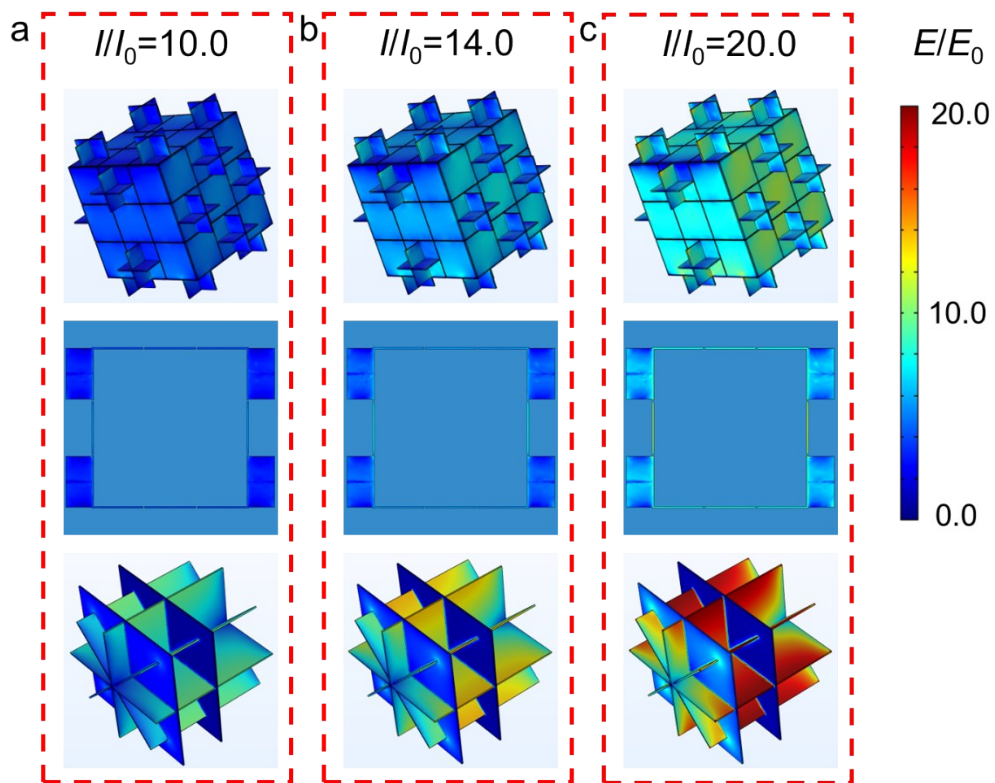
Figure S10. Electric field intensity distributions for NCMO and MO models at current densities of (a) $10I_0$, (b) $14I_0$, and (c) $20I_0$.
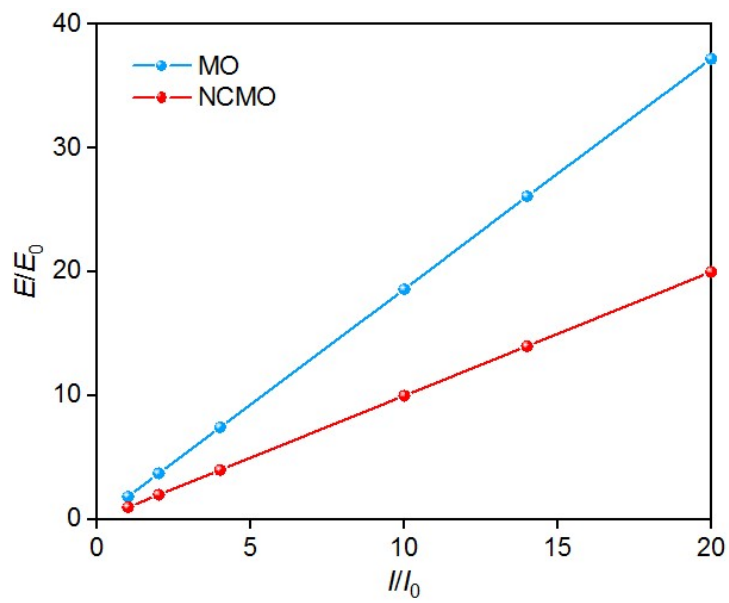
Figure S11. The maximum electric field intensities for MO and NCMO models at

different current densities.
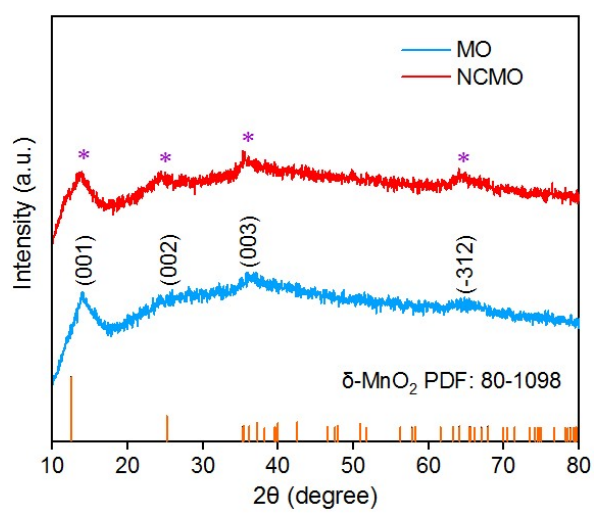
Figure S12. X-ray diffraction patterns of NCMO.
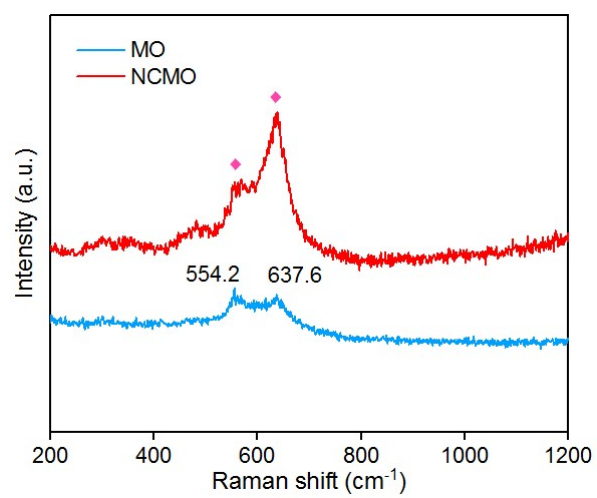
Figure S13. Raman spectra of NCMO and pure MnO_2 samples.
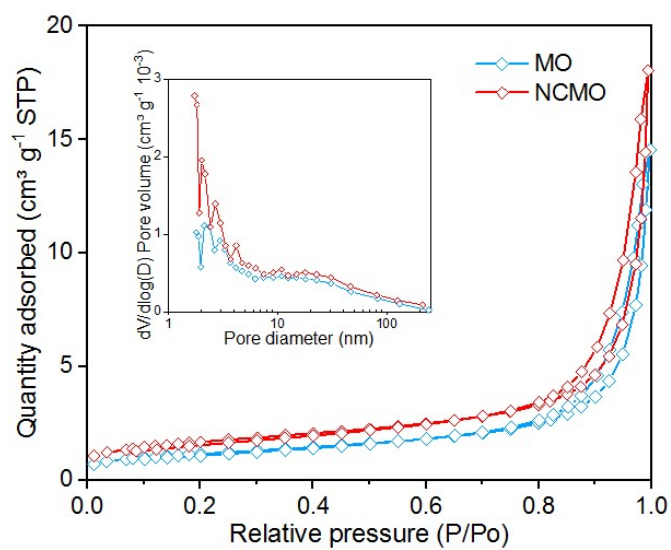
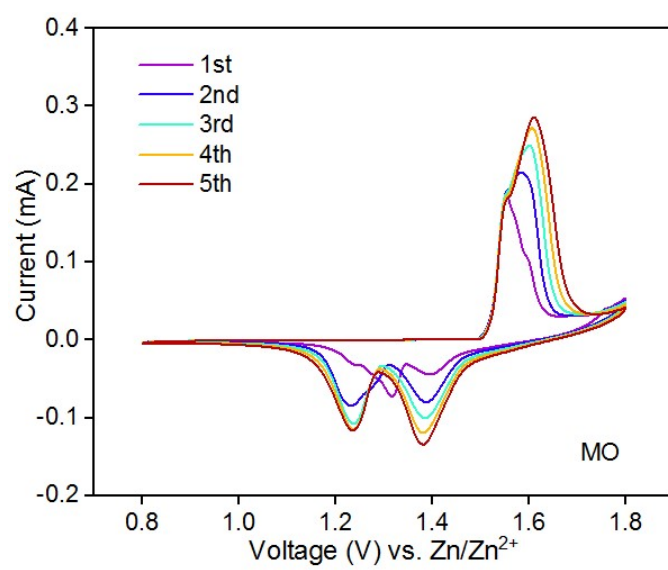**Figure S14.** N_2 adsorption–desorption isotherms (inset: pore-size distribution) of the

NCMO sample.
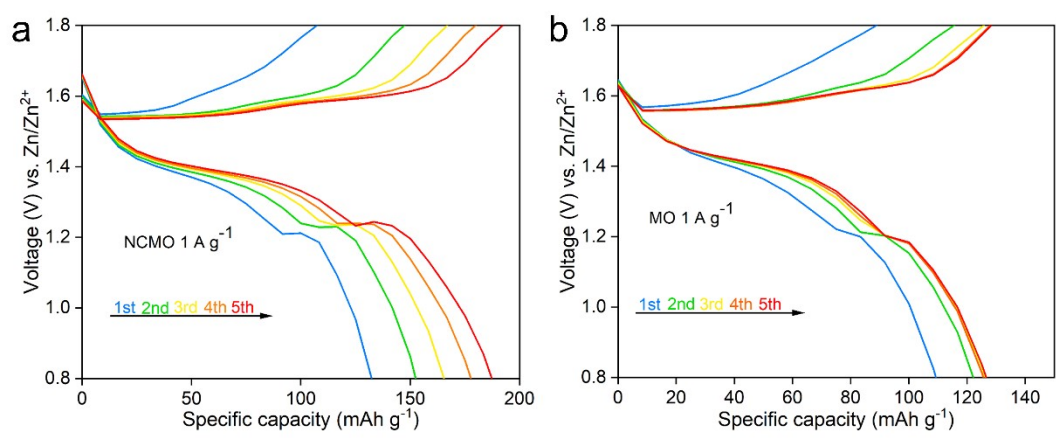
Figure S15. Cyclic voltammetry curves of pristine MnO$_2$.

Figure S16. Galvanostatic charge–discharge profiles of NCMO (a) and pristine MnO_2 samples (b).
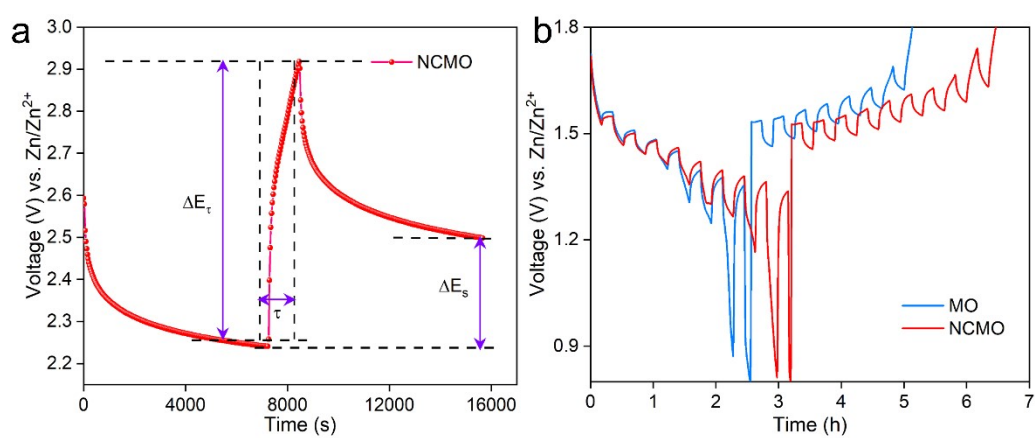
Figure S17. a) Diagram of the galvanostatic intermittent titration technique (GITT) procedure (a single current pulse was applied for 10 min, followed by an open-circuit stand for 600 s). b) GITT curves of NCMO.

Table S1. Adsorption energies of Zn in MO and NCMO.

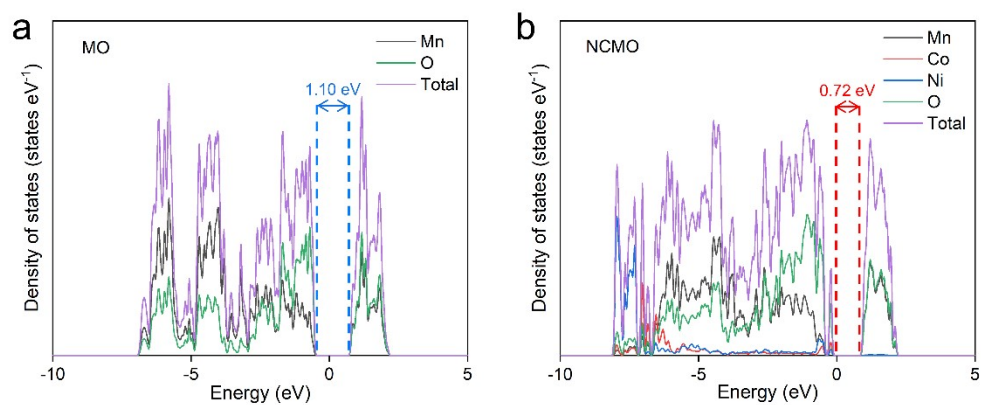| Energy (eV)	sub	Zn	sub+Zn	adsorption energy
Zn-MO	-514.70	-1.56	-518.51	-2.25
Zn-NCMO	-470.09	-1.56	-473.60	-1.95

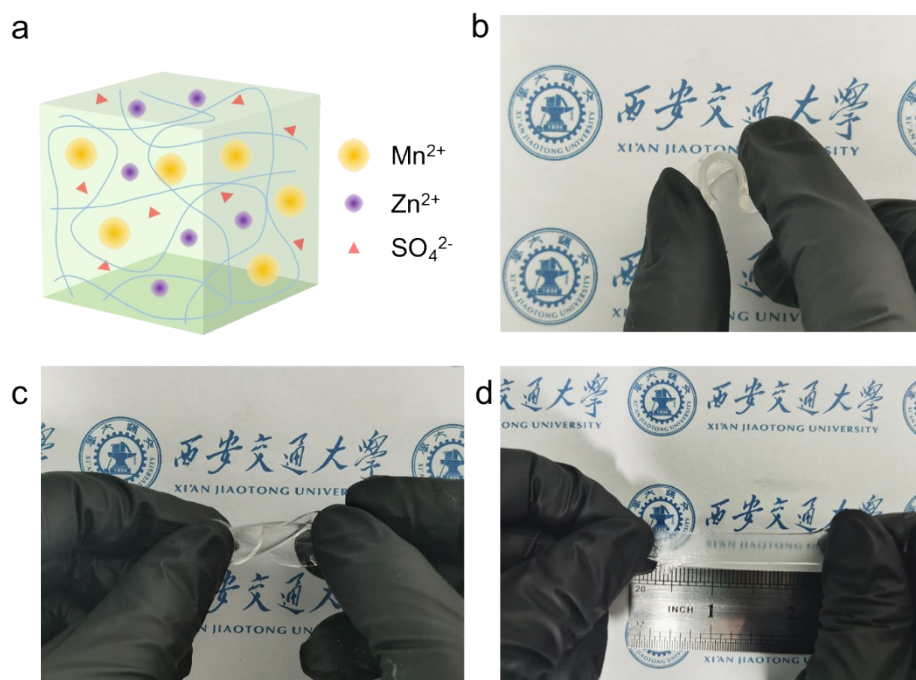**Figure S18.** Partial density of states of (a) MO and (b) NCMO.

Figure S19. a) Illustration of a quasi-solid-state PAM/ZnSO$_4$–MnSO$_4$–glucose gel. The mechanical flexibility test of the quasi-solid-state gel: bending (b), twisting (c), and stretching (d).
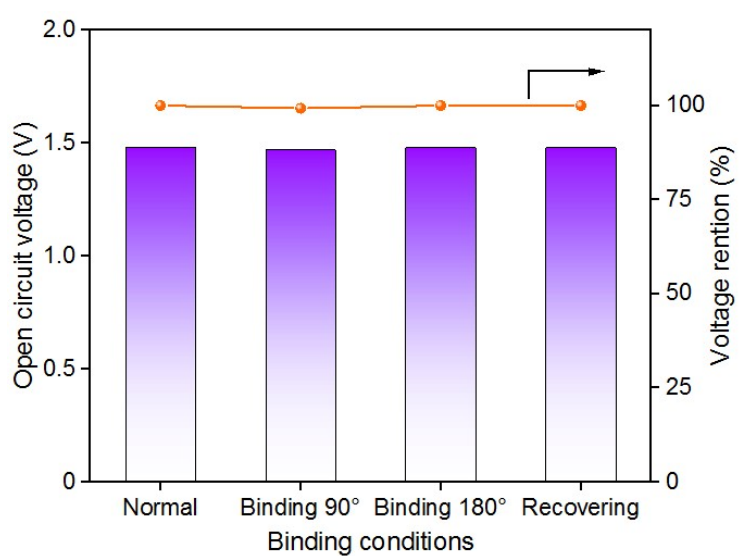
Figure S20. Open-circuit voltages of flexible quasi-solid-state NCMO//Zn cells at
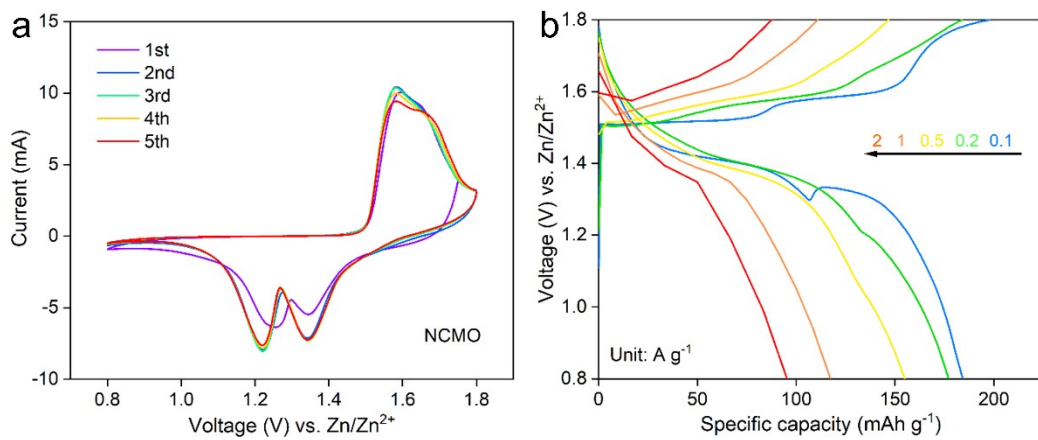
different states.

Figure S21. Electrochemical properties of flexible quasi-solid-state NCMO//Zn cells.

a) The initial five cyclic voltammetry curves of NCMO//Zn cells. b) The rate

performance of NCMO//Zn cells.

Reference:

[1]   Y. Gao, J. Yin, X. Xu, Y. H. Cheng, *J. Mater. Chem. A* **2022**, 10, 9773.

[2]   B. E. Conway, V. Birss, J. Wojtowicz, *J. Power Sources* **1997**, 66, 1.

[3]   Z. Gan, J. Yin, X. Xu, Y. Cheng, T. Yu, *ACS Nano* **2022**, 16, 5131.

[4]   Y. Gao, X. Wang, J. Ma, Z. Wang, L. Chen, *Chem. Mater.* **2015**, 27, 3456.

[5]   S. Selcuk, A. Selloni, *J. Phys. Chem. C* **2015**, 119, 9973.

[6]   H. Chen, C. L. Freeman, J. H. Harding, *Phys. Rev. B* **2011**, 84, 085108.